Journal of Fluids and Structures 107 (2021) 103415

Contents lists available at ScienceDirect

Journal of Fluids and Structures

journal homepage: www.elsevier.com/locate/jfs

Numerical study on vortex-induced vibration of circular cylinder with two-degree-of-freedom and geometrical nonlinear system

Tian Li [a,b], Takeshi Ishihara [b,*]

[a] School of Civil Engineering, Chongqing University, Chongqing, 400044, China
[b] Department of Civil Engineering, School of Engineering, The University of Tokyo, Tokyo, 113-8656, Japan

ARTICLE INFO

Article history:
Received 4 April 2021
Received in revised form 12 October 2021
Accepted 12 October 2021
Available online xxxx

Keywords:
Vortex-induced vibration
Circular cylinder
Two-degree-of-freedom
Geometrical nonlinearity
SST k-ω turbulence model
Large eddy simulation

ABSTRACT

The vortex-induced vibration (VIV) of circular cylinder in uniform flow with two-degree-of-freedom (2DOF) and geometrical nonlinear system is investigated numerically using the combined sliding and layering dynamic meshes. The characteristics of vibration amplitude, fluid force coefficients, branching behaviour, vibration trajectory, energy transfer and flow pattern of circular cylinder in VIV are studied with two-dimensional shear stress transfer (SST) k-ω turbulence model and three-dimensional large eddy simulation (LES). It is found that in the simulation with LES model the predicted vibration amplitude and fluid force coefficients show good agreement with the experimental data, while in the simulation with SST k-ω model these parameters are significantly underestimated. The two triplets (2T) vortex shedding mode happens in the super upper branch of circular cylinder with 2DOF linear system and leads the large-magnitude positive energy transferring from fluid to cylinder, which causes the maximum vibration amplitude. For the circular cylinder with 2DOF nonlinear system, the vibration simulated by LES model shows a galloping-like phenomenon that the amplitude keeps increasing with the reduced velocity U_r. The crescent-shaped trajectory and the 2T vortex shedding mode happen upon the critical U_r, which is similar to that in the super upper branch of circular cylinder with 2DOF linear system. This phenomenon is caused by the amplitude-dependent stiffness of nonlinear system and the modified reduced velocity U^* reveals the universality of vibration amplitude for the circular cylinders with linear and nonlinear systems.

1. Introduction

When a circular cylinder is immersed into a steady flow, vortices shed from alternating sides of the cylinder and lead the unsteady drag and lift forces on the cylinder. These vortices may induce significant vibration when the vortex-shedding frequency f_v approaches the structural natural frequency f_n, which is called the vortex-induced vibration (VIV). VIV is an important concern for engineering applications, such as bridge cables subjected to wind and offshore risers subjected to ocean currents. It may increase the dynamic load on the structures and accelerate the fatigue failure. For the positive aspect, the large-amplitude VIV is considered for energy harvesting in recent years as a pure, plenty and sustainable energy resource (Bernitsas et al., 2008).

* Corresponding author.
E-mail address: ishihara@bridge.t.u-tokyo.ac.jp (T. Ishihara).

https://doi.org/10.1016/j.jfluidstructs.2021.103415
0889-9746/

Although the VIV of flexible circular cylinder is essentially a three-dimensional (3D) phenomenon, the end effect and multiple vibration modes are negligible for the stiff structures, therefore it can be simplified as a two-degree-of-freedom (2DOF) system that a rigid circular cylinder elastically mounted in the streamwise and transverse directions. In addition, the vibration amplitude of VIV in the transverse direction is generally much larger than that in the streamwise direction, so that the study of VIV started from the canonical problem of a rigid circular cylinder freely vibrating in the transverse direction as a single-degree-of-freedom (SDOF) system. The wind tunnel experiment of Feng (1968) is one of the earliest and widely known studies for the VIV of circular cylinder with SDOF system. It was found that the maximum VIV amplitude of cylinder decreased as the structural damping ratio $\zeta = c/(2m\omega_n)$ increased, where c, m and ω_n are the damping, mass and natural angular frequency of structure. Khalak and Williamson (1996, 1997, 1999) conducted a comprehensive study for the SDOF VIV of circular cylinder through water tank tests. Their results support the theory of Griffin (1980) that the maximum VIV amplitude of circular cylinder depends on the mass-damping ratio $m^*\zeta$, where the mass ratio $m^* = 4m/(\pi\rho D^2 L)$ is the ratio of structure mass m to the displaced fluid mass, with D and L being the diameter and length of circular cylinder and ρ being the fluid density. In their research with $m^* = 2.4$ and 10.3, three branches of response depending on the reduced velocity U_r were found, namely the initial branch, upper branch and lower branch, where U_r equals U/f_nD with U being the freestream velocity, while in Feng's research with $m^* = 248$ only the initial branch and lower branch existed and the upper branch was not observed. Khalak and Williamson (1999) showed that different modes of vortex shedding were directly associated with these branches. The 2S mode indicating two single opposing-sign (counter-rotating) vortices shedding per vibration period happened in the initial branch and the 2P mode indicating two pairs of opposing-sign vortices shedding per vibration period happened in the upper and lower branches, follows the terminologies of vortex shedding mode defined by Williamson and Roshko (1988).

Furthermore, the addition of vibration in the streamwise direction forms the 2DOF VIV of circular cylinder. Jauvtis and Williamson (2004) found for the case of the mass ratio $m^* > 6.0$, the system response branches, peak amplitudes and vortex shedding modes of circular cylinder with 2DOF system were similar to those with the SDOF system. However, for $m^* < 6.0$, a high-amplitude branch of response named as super-upper branch was induced after adding the streamwise degree of freedom in the system of circular cylinder. They also showed that the emergence of the super-upper branch was related to the arising of the 2T vortex formation mode, where two triplets of vortices shed per oscillation period. The 2T and multi-vortex shedding modes were also found to relate with the appearance of a third and higher harmonics in the lift force.

To investigate detailed characteristics and the mechanism of VIV, the numerical simulation allowing a coupled analysis of the fluid–structure interaction is considered as a powerful tool. It provides a simultaneous vision of the wake patterns, fluid forces and dynamic responses. The numerical studies on the VIV of circular cylinders were conducted for SDOF system with low Reynolds number Re in the early stage, where Re is defined as $\rho UD/\mu$ with μ standing for the dynamic viscosity of fluid. Leontini et al. (2006) and Willden and Graham (2006) investigated the branching behaviour of SDOF VIV using two-dimensional (2D) Navier Stokes simulation at $Re = 200$ and 50 to 400 respectively. The direct numerical simulation (DNS) studies were conducted by Lucor et al. (2005) and Zhao et al. (2014) with Re up to 3000 and 1000 respectively using 3D models. These numerical results agreed with the experimental phenomena qualitatively, while the predicted vibration amplitudes were not comparable with the experimental data because most of experiments were performed at the subcritical Reynolds number. Guilmineau and Queutey (2004) performed numerical simulation for the VIV of a circular cylinder with SDOF system by using 2D shear stress transport (SST) k-ω turbulence model with Reynolds number up to 15 000, which well captured the responses in the initial and lower branches, but the response in the upper branch did not correspond with the experimental data. The same problem was found by Pan et al. (2007) which may be due to the limitation of 2D numerical simulation because the three-dimensionality of flow in the wake of a circular cylinder is significant when the Reynolds number exceeds 200 (Williamson, 1988). Zhao et al. (2014) found the three-dimensionality of flow was strong in the upper branch and indicated the necessity of three-dimensional simulation. Saltara et al. (2011) simulated the VIV of a SDOF circular cylinder with a low mass-damping parameter at $Re = 10\,000$ using detached eddy simulation (DES). Their numerical simulations for $U_r < 6$ agreed with the experimental results of Khalak and Williamson (1997) while the vibration amplitudes and force coefficients were overestimated for $U_r > 6$. Recently, Ishihara and Li (2020) investigated the VIV of a SDOF circular cylinder with a large mass ratio of 248 and a small damping ratio of 0.00257 at the Reynolds numbers ranging from 16 000 to 24 500 using large eddy simulation (LES). The predicted vibration amplitude and frequency agreed well with the experimental data of Feng (1968).

Besides the numerical studies for the VIV of circular cylinder with SDOF system, a few numerical studies were performed for the circular cylinder with 2DOF system. Pontaza and Chen (2007) employed 3D LES method to study VIV of a 2DOF circular cylinder with low structural mass and damping at $Re = 10^5$ for the case of $U_r = 6$ only. A response characterized by the figure-eight pattern was observed and the vortex shedding with 2S mode was exhibited. However, the super upper branch with 2T mode shown in the experiment was not investigated, which was also not reproduced by 2D numerical simulations of Singh and Mittal (2005), Zhao and Cheng (2011) and Wang et al. (2019). Navrose and Mittal (2013) conducted the DNS numerical study for the VIV of 2DOF circular cylinder at $Re = 1000$ without the validation by experimental data. Gsell et al. (2016) examined the VIV of a 2DOF circular cylinder at $Re = 3900$ also using DNS method and the predicted responses of circular cylinder were underestimated comparing with the experimental data reported by Jauvtis and Williamson (2004) since the simulation was performed at a lower Reynolds number than the experimental one. Until now, the numerical study for the VIV of 2DOF circular cylinder is still limited.

As the VIV amplitude of 2DOF circular cylinder can achieve times of cylinder diameter with low $m^*\zeta$, the axial stretching of the springs may become intrinsically nonlinear, amplitude-dependent and bi-directionally coupled (Srinil and Zanganeh, 2012). Even though, most of previous research disregarded the effect of geometrical nonlinearities on the VIV of circular cylinder. Mackowski and Williamson (2013) performed an experiment for the VIV of circular cylinder with nonlinear restoring forces using the Cyber–Physical Fluid Dynamics force-feedback technique. They found that the vibration amplitude increased as the nonlinear restoring force increased and showed a galloping-like vibration. However, the mechanism of this phenomenon has not been clarified yet.

In this study, the vortex-induced vibration of circular cylinder with 2DOF and geometrical nonlinear system is investigated using 2D SST k-ω and 3D LES turbulence models. The numerical models for the flow and structure are described in Section 2. The numerical results for the VIV of circular cylinder with 2DOF linear system are discussed in Section 3. The effect of geometrical nonlinear system on the VIV of circular cylinder is investigated in Section 4. The conclusions are summarized in Section 5.

2. Numerical models

The numerical models used in this study are explained in this section. The governing equations and solution schemes are given in Section 2.1. The modelling of oscillation system is introduced in Section 2.2 and the computational domain and mesh are described in Section 2.3.

2.1. Governing equations and schemes

The turbulence model is important to simulate the bluff body aerodynamics at high Reynolds number accurately and economically. The SST k-ω and LES models are chosen for the 2D and 3D simulations respectively in this study because of their good performance for simulating the phenomena with strong flow separation and pressure gradient (Ferziger and Peric, 2002; Li et al., 2018). In the SST k-ω model, the turbulence within every time step is averaged out and parameterized. In the LES analysis, large eddies are directly computed in simulations, while the influence of eddies smaller than the control volume are parameterized. The governing equations for the averaged or filtered continuity and unsteady incompressible Navier–Stokes equations in the moving mesh system are

$$\frac{\partial \rho \tilde{u}_i}{\partial x_i} = 0 \tag{1}$$

$$\rho \frac{\partial \tilde{u}_i}{\partial t} + \rho \frac{\partial \tilde{u}_i}{\partial x_j}\left(\tilde{u}_j - \hat{u}_j\right) = -\frac{\partial \tilde{p}}{\partial x_i} + \mu \frac{\partial}{\partial x_j}\left(\frac{\partial \tilde{u}_i}{\partial x_j} + \frac{\partial \tilde{u}_j}{\partial x_i}\right) - \frac{\partial \tau_{ij}}{\partial x_j} \tag{2}$$

where x is the coordinate, u is the velocity, p is the pressure and t is the time. The subscripts i, j and k stand for different directions in the Cartesian coordinates, namely the streamwise, transverse and vertical directions. The superscript "$\sim$" indicates time averaged values in the simulation with SST k-ω model, while it indicates the resolved values in the simulation with LES model. $\hat{u}$ is the velocity component of the moving mesh. τ_{ij} is introduced to consider the difference between $\widetilde{u_i u_j}$ and $\tilde{u}_i \tilde{u}_j$, i.e.,

$$\tau_{ij} = \rho \widetilde{u_i u_j} - \rho \tilde{u}_i \tilde{u}_j \tag{3}$$

Although the expressions of τ_{ij} in the SST k-ω and LES models are same, their meanings are different. τ_{ij} in the SST k-ω model is the time-averaged Reynolds stress and stands for the effect from the vortices to the mean flow field, while τ_{ij} in LES model indicates the subgrid-scale Reynolds stress and accounts for the contribution from the unresolved smaller vortices to the large size vortices.

The time-averaged Reynolds stress τ_{ij} in the SST k-ω model is modelled as

$$\tau_{ij} = -2\mu_t \tilde{S}_{ij} + \frac{2}{3}(\rho k + \mu_t \frac{\partial \tilde{u}_k}{\partial x_k})\delta_{ij} \tag{4}$$

where δ_{ij} is the Kronecker delta and $\tilde{S}_{ij}$ is the rate-of-strain tensor, i.e., the symmetric component of the velocity gradient tensor $\nabla \tilde{u}$ defined as

$$\tilde{S}_{ij} = \frac{1}{2}\left(\frac{\partial \tilde{u}_i}{\partial x_j} + \frac{\partial \tilde{u}_j}{\partial x_i}\right) \tag{5}$$

μ_t is the turbulent viscosity and is modelled as (Menter, 1994)

$$\mu_t = \rho \frac{k}{\omega} \tag{6}$$

where k is the turbulence kinetic energy and ω is the turbulence frequency.

In the LES turbulence model, the subgrid-scale stress is modelled as

$$\tau_{ij} = -2\mu_t \tilde{S}_{ij} + \frac{1}{3}\tau_{kk}\delta_{ij} \tag{7}$$

Table 1
Structural parameters in the water.

U_r	m^*	ζ	$m^*\zeta$	Re	f_n (Hz)	D (m)
2–14	2.6	0.0036	0.009	2000–14 000	0.4	0.05

where μ_t is the subgrid-scale turbulent viscosity and modelled by the dynamic Smagorinsky–Lilly model (Smagorinsky, 1963; Germano et al., 1991; Lilly, 1992) as

$$\mu_t = \rho L_s^2 \left|\tilde{S}\right| = \rho L_s^2 \sqrt{2\tilde{S}_{ij}\tilde{S}_{ij}} \tag{8}$$

where $\left|\tilde{S}\right| = \sqrt{2\tilde{S}_{ij}\tilde{S}_{ij}}$ and L_s is the mixing length of subgrid-scales defined as

$$L_s = min\left(\kappa d^*, C_s V^{\frac{1}{3}}\right) \tag{9}$$

where κ is the von Karman constant and is taken equal to 0.42. C_s is Smagorinsky constant, which is dynamically computed based on the information provided by the resolved scales of motion (ANSYS Inc., 2015). d^* is the distance to the closest wall, and V is the volume of a computational cell.

For the wall-adjacent cells, when they are in the laminar sub-layer, the wall shear stress is obtained from the laminar stress–strain relationship as

$$\frac{\tilde{u}}{u_\tau} = \frac{\rho u_\tau y^*}{\mu} \tag{10}$$

where $\tilde{u}$ is the filtered velocity that is tangential to the wall, u_τ is the friction velocity and y^* is the distance between the centre of the cell and the wall. If the mesh cannot resolve the laminar sub-layer, it is assumed that the centroid of the wall-adjacent cells falls within the logarithmic region of the boundary layer, and the law-of-the-wall is employed as

$$\frac{\tilde{u}}{u_\tau} = \frac{1}{\kappa} ln\ E\left(\frac{\rho u_\tau y^*}{\mu}\right) \tag{11}$$

where the constant E is taken equal to 9.8.

The averaged or filtered Navier–Stokes equations are solved by the commercial CFD code ANSYS Fluent 16.2 (ANSYS Inc., 2015) using the finite volume method. The second-order difference scheme is used for the convective and viscosity terms. SIMPLE (Semi-Implicit Method for Pressure Linked Equations) algorithm is employed for solving the discretized equations. The simulations were performed on the parallel computing cluster system (Intel Xeon CPU E5-2667 v4, 240 cores, 960 GB memory). The 3D LES simulation with 80 cores takes about 150 h of wall-clock-time and the 2D SST k-ω simulation with 8 cores takes about 30 h of wall-clock-time for each reduced velocity.

2.2. Structural dynamic model

The 2DOF dynamic system of circular cylinder is modelled by a mass–spring system in both streamwise and transverse directions considering the geometrical nonlinearity as

$$m\ddot{x} + c\dot{x} + kx\left[1 + \alpha_x(\frac{x}{D})^2 + \beta_x(\frac{y}{D})^2\right] = F_D(t) \tag{12}$$

$$m\ddot{y} + c\dot{y} + ky\left[1 + \alpha_y(\frac{x}{D})^2 + \beta_y(\frac{y}{D})^2\right] = F_L(t) \tag{13}$$

where F_D and F_L are the drag and lift forces obtained by integrating pressure and friction over the cylinder surface. k is the structural stiffness and the nonlinear coupled restoring force is considered based on the model of Bush (1992). α and β are the geometrical nonlinear coefficients caused by the amplitude-dependency and bi-directionally coupling of spring stiffness. The subscript x and y stand for the streamwise and transverse direction respectively. These geometrical nonlinear coefficients are derived through the Duffing equation described by Bush (1992) in a one-directional spring case as shown in Appendix. $\alpha_x = \alpha_y = \beta_x = \beta_y = 0.7$ were used in Srinil and Zanganeh (2012) as the best setting of these geometrical nonlinear coefficients through their theoretical study and are used in this study. Specially, this dynamic system becomes linear when $\alpha_x = \alpha_y = \beta_x = \beta_y = 0$ and turns to SDOF if only one equation of motion is taken into account.

The structural parameters are set the same as the water tank experiment of Jauvtis and Williamson (2004) in the present numerical models. The detail setting of structural parameters is shown in Table 1, where the ζ and f_n are the ones in the water. The added mass is considered for ζ and f_n using the definitions in Jauvtis and Williamson (2004) as $\zeta = \frac{c}{2\sqrt{k(m+m_A)}}$ and $f_n = \frac{1}{2\pi}\sqrt{\frac{k}{m+m_A}}$, where m_A is the added mass and equals to the mass of displaced water. To analyse the structural response of the dynamic system, the equation of motion is solved by the fourth-order Runge–Kutta method.

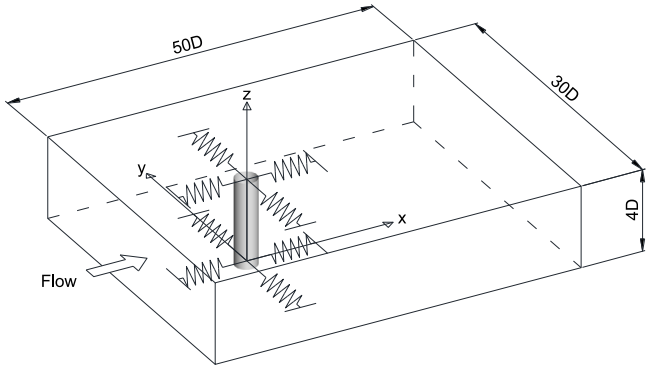

Fig. 1. Schematic of computational domain.

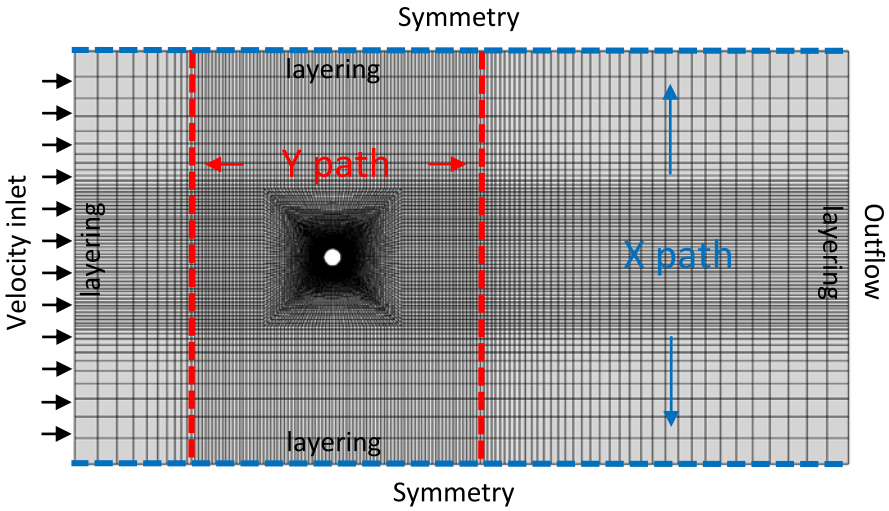

Fig. 2. Numerical mesh and boundary conditions.

2.3. Computational domain and mesh

The schematic of computational domain is shown in Fig. 1. The width and depth of the computational domain are 50*D* and 30*D* respectively and the spanwise length *L* of the computational domain in LES study is 4*D*, referred to the previous research of Ishihara and Li (2020) and Li and Ishihara (2021) that this length is enough to simulate the lift correlation in the spanwise direction of circular cylinder. The cylinder is located 15*D* downstream from the inlet. The computational domain used in the simulation with SST k-ω model is two-dimensional.

The numerical mesh and boundary conditions are shown in Fig. 2 that the hexahedron mesh is used with high resolution near the cylinder to capture the flow accurately. The $y+$ value of the near-wall mesh is less than 1. Uniform velocity condition is specified at the inlet boundary, and zero diffusive outflow condition is used at the outlet boundary. Symmetric condition is used for the transverse and vertical surfaces of domain. The influence of symmetric and periodic transverse boundaries for the transverse side surfaces of domain is compared in Ishihara and Li (2020) and it is found the correlation coefficient of lift force along the spanwise direction of circular cylinder is better simulated with symmetric boundary than periodic boundary.

The computational domain is divided into three subdomains combined with sliding and layering meshes, which is special designed for this study to satisfy the requirement of computational accuracy and flexibility. The inside domain between the two vertical sliding interfaces moves in both transverse and streamwise directions, and the domain outside the two vertical interfaces deforms in the streamwise direction with the dynamic layering mesh applied in the inlet and outlet boundaries. The sliding mesh is a special case of general dynamic mesh wherein the nodes move rigidly in a given dynamic mesh zone. Multiple cells are connected with each other through non-conformal interfaces. As the mesh motion is updated in time, the non-conformal interfaces are likewise updated to reflect the new position of each zone. The flux across the non-conformal interfaces is estimated considering the two adjoining cells that move relatively to each other (Sarwar and Ishihara, 2010). In the region using the layering mesh, both split and collapse factors for the cell near the

Table 2
Mesh convergence test.

	Mesh quantity	A_x/D	A_y/D
Mesh 1	455,680	0.3156	1.3576
Mesh 2	911,360	0.3163 (0.2%)	1.4146 (4.2%)
Mesh 3	1,822,720	0.3149 (0.4%)	1.4458 (2.2%)

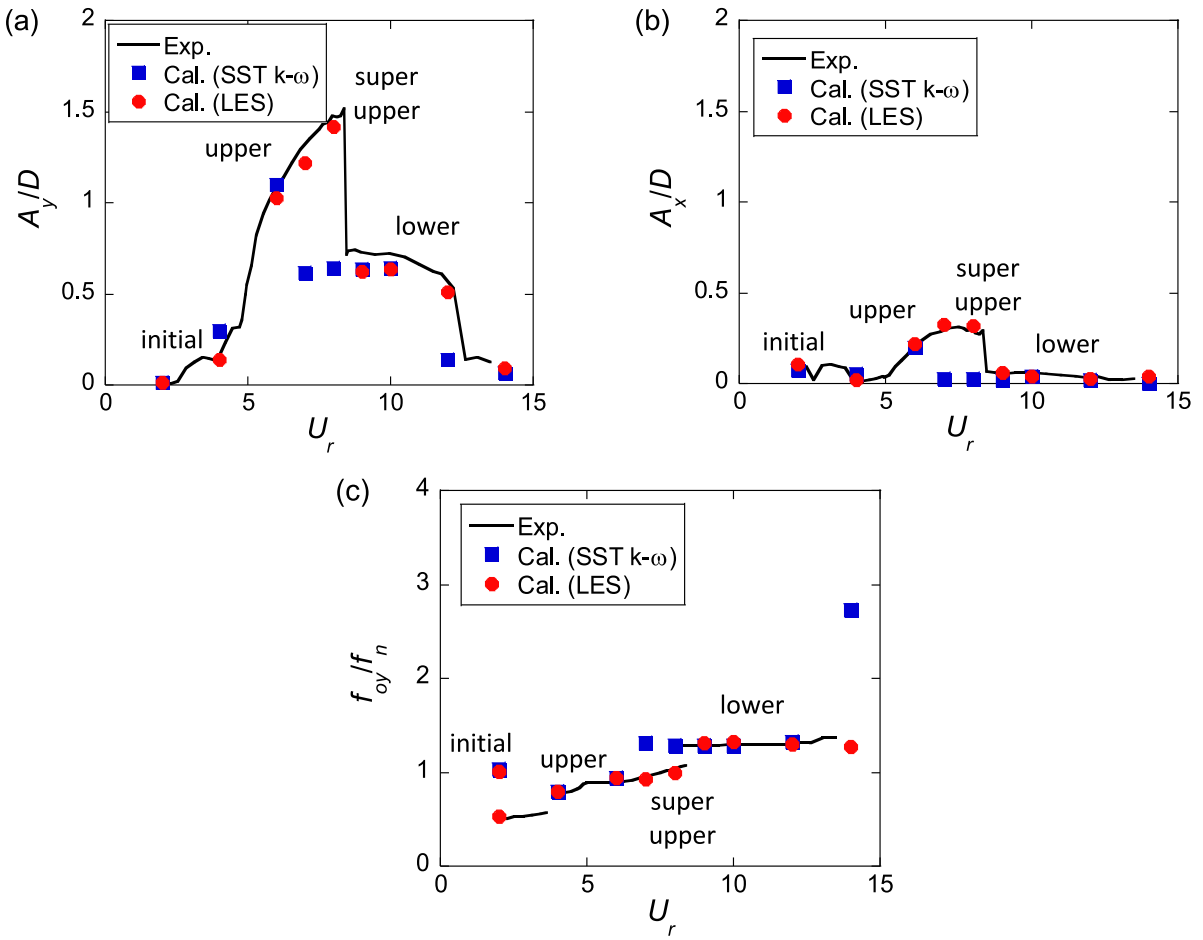

Fig. 3. Variation of (a) non-dimensional transverse amplitude A_y/D, (b) non-dimensional streamwise amplitude A_x/D and (c) non-dimensional transverse frequency f_{oy}/f_n of free vibration with U_r for circular cylinder with 2DOF linear system.

boundaries are 0.4 with respect to the first cell height at the boundaries referred to Zhang and Ishihara (2018). The sliding mesh has the second order accuracy, which is higher than the dynamic layer mesh with the first order accuracy as shown in Ferziger and Peric (2002). The dynamic layer mesh is highly flexible and is used in the domain where the flow field is almost uniform and changes slowly to reduce its adverse effect on the numerical accuracy.

The convergence of mesh is tested through the predicted vibration amplitude of circular cylinder at $U_r = 8$, corresponding to the maximum amplitude of VIV in the experiment by Jauvtis and Williamson (2004). The non-dimensional streamwise vibration amplitude A_x/D and transverse vibration amplitude A_y/D of circular cylinder simulated by LES model are shown in Table 2, where A is the dimensional vibration amplitude equalling $\sqrt{2}$ times of the standard deviation of displacement. The mesh resolution increases gradually from Mesh 1 to Mesh 3 and the change ratio of result is shown in brackets. It is noticed that the difference of predicted vibration amplitudes between Mesh 2 and Mesh 3 is less than 3%, which is acceptable for the convergence criterion of engineering applications. Thus, Mesh 2 is used in the following simulations in consideration of both accuracy and efficiency.

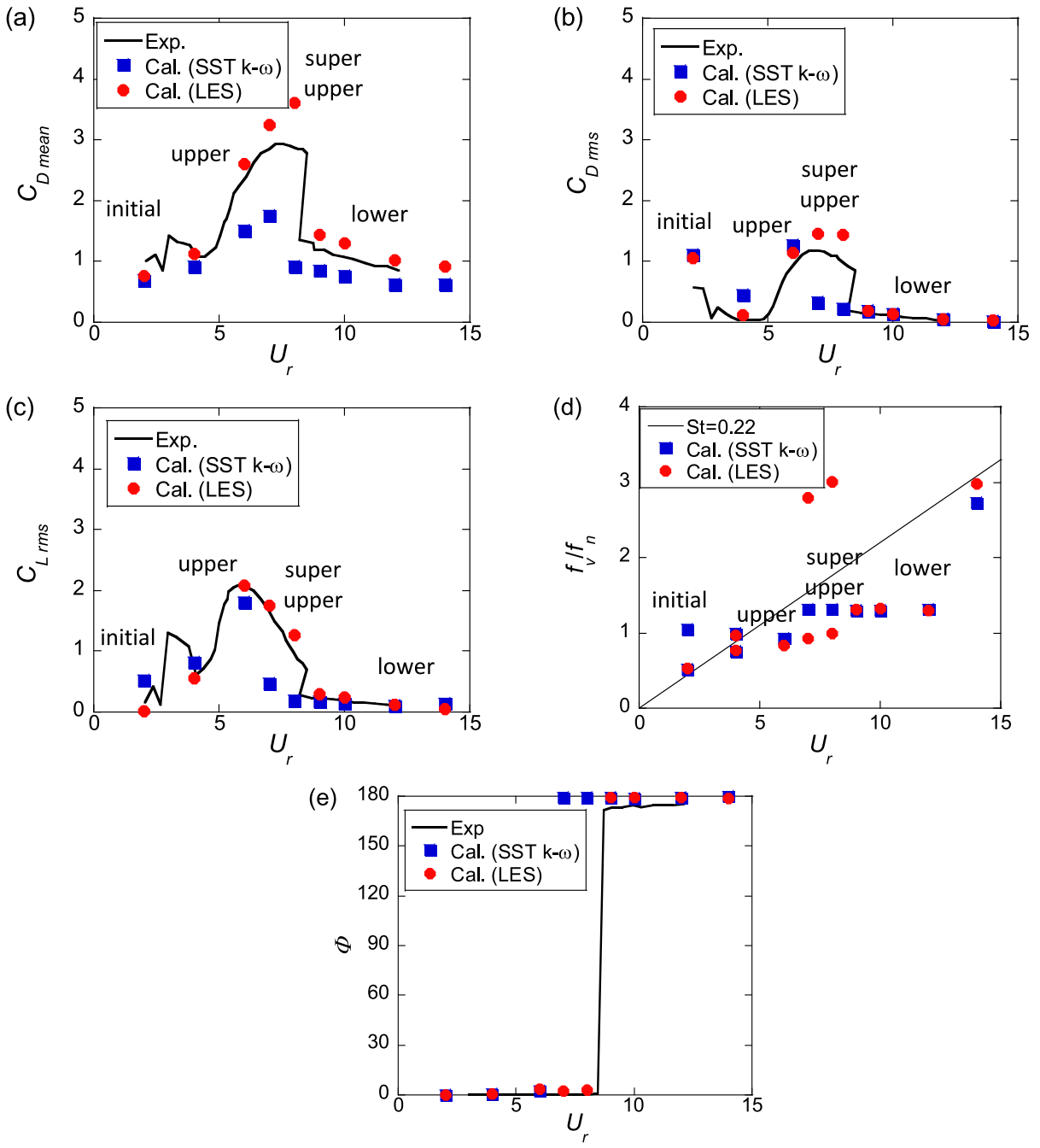

Fig. 4. Variation of (a) mean drag coefficients $C_{D\ mean}$, (b) fluctuating drag coefficients $C_{D\,rms}$, (c) fluctuating lift coefficients $C_{L\,rms}$, (d) non-dimensional vortex shedding frequency f_v/f_n and (e) phase angle Φ between lift force and transverse displacement with U_r for the circular cylinder with 2DOF linear system.

3. VIV of circular cylinder with 2DOF linear system

The free-vibration of circular cylinder with 2DOF linear system under the reduced velocity U_r from 2 to 14 is simulated by increasing U_r with a step of 2. A smaller step of 1 is used near the resonance velocity $U_r = 6\sim10$ to catch the characteristics of VIV more clearly. Both f_n and D are fixed while U is varied to change U_r in this series of simulations, resulting in $Re = 2000\sim14\,000$, which is same as the experiment setting of Jauvtis and Williamson (2004). The oscillation under each U_r is simulated for over 50 periods to get reasonable statistics. The predicted non-dimensional transverse and

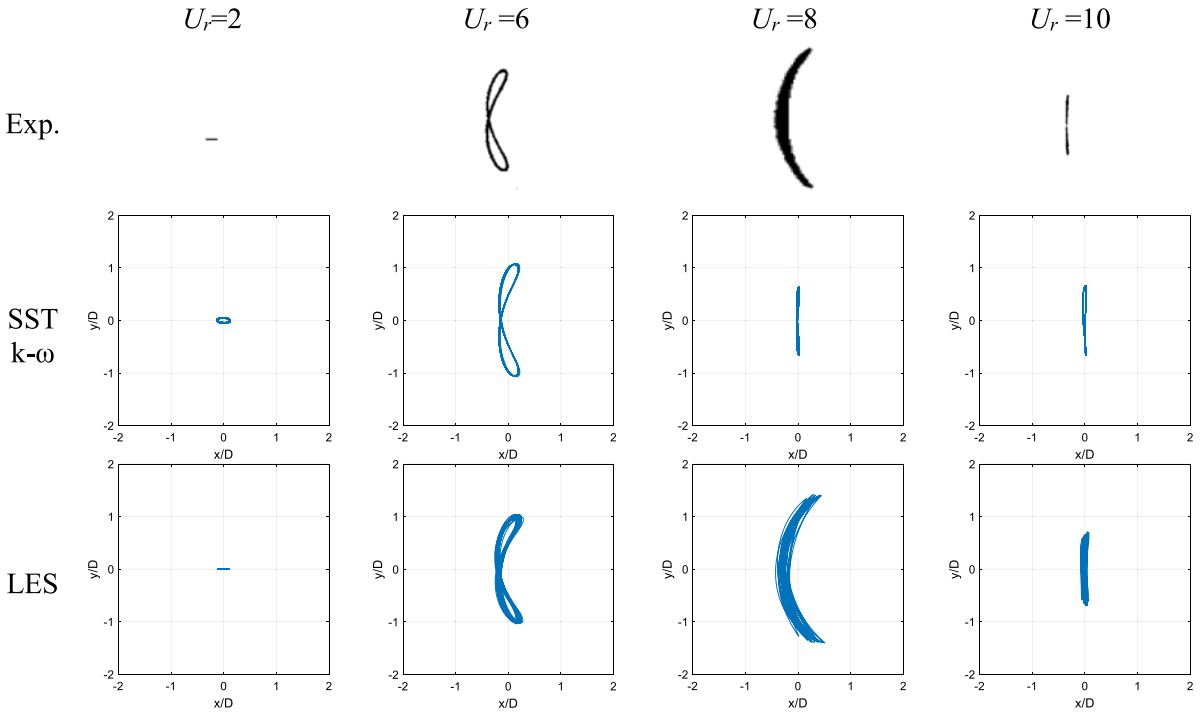

Fig. 5. Vibration trajectory of circular cylinder with 2DOF linear system.

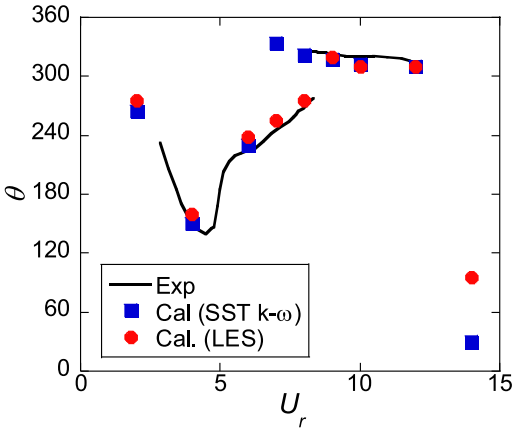

Fig. 6. Phase angles between streamwise and transverse motion.

streamwise vibration amplitudes A_y/D and A_x/D as well as the non-dimensional transverse vibration frequency f_{oy}/f_n by k-ω model and LES model are shown in Fig. 3 compared with the experimental data of Jauvtis and Williamson (2004). It is noticed that the vibration amplitude of circular cylinder firstly increases slightly at $U_r = 2\sim4$, which belongs to the initial branch. Then the vibration amplitude increases rapidly and gets its peak at $U_r = 8$. The increasing part include upper and super upper branches distinguished by the vortex shedding mode which will be discussed later. After that the amplitude decreases sharply at $U_r = 8\sim9$. Finally, the amplitude decreases gradually at $U_r = 9\sim14$, which belongs to the lower branch. The trends of vibration amplitude for both transverse and streamwise directions are similar while the transverse vibration is much more significant than the streamwise one. The vibration frequency in the transverse direction f_{oy} has two dominating values corresponding to the structure natural frequency and the vortex shedding frequency of fixed cylinder at $U_r = 2$. The former one is neglected in the experimental results of Jauvtis and Williamson (2004), but shown in Khalak and Williamson (1999). f_{oy} generally increases with the reduced velocity U_r and is separated for different branches. The maximum vibration amplitude and the critical reduced velocity of transition from super upper branch to lower branch are underestimated by SST k-ω model but well predicted by LES model.

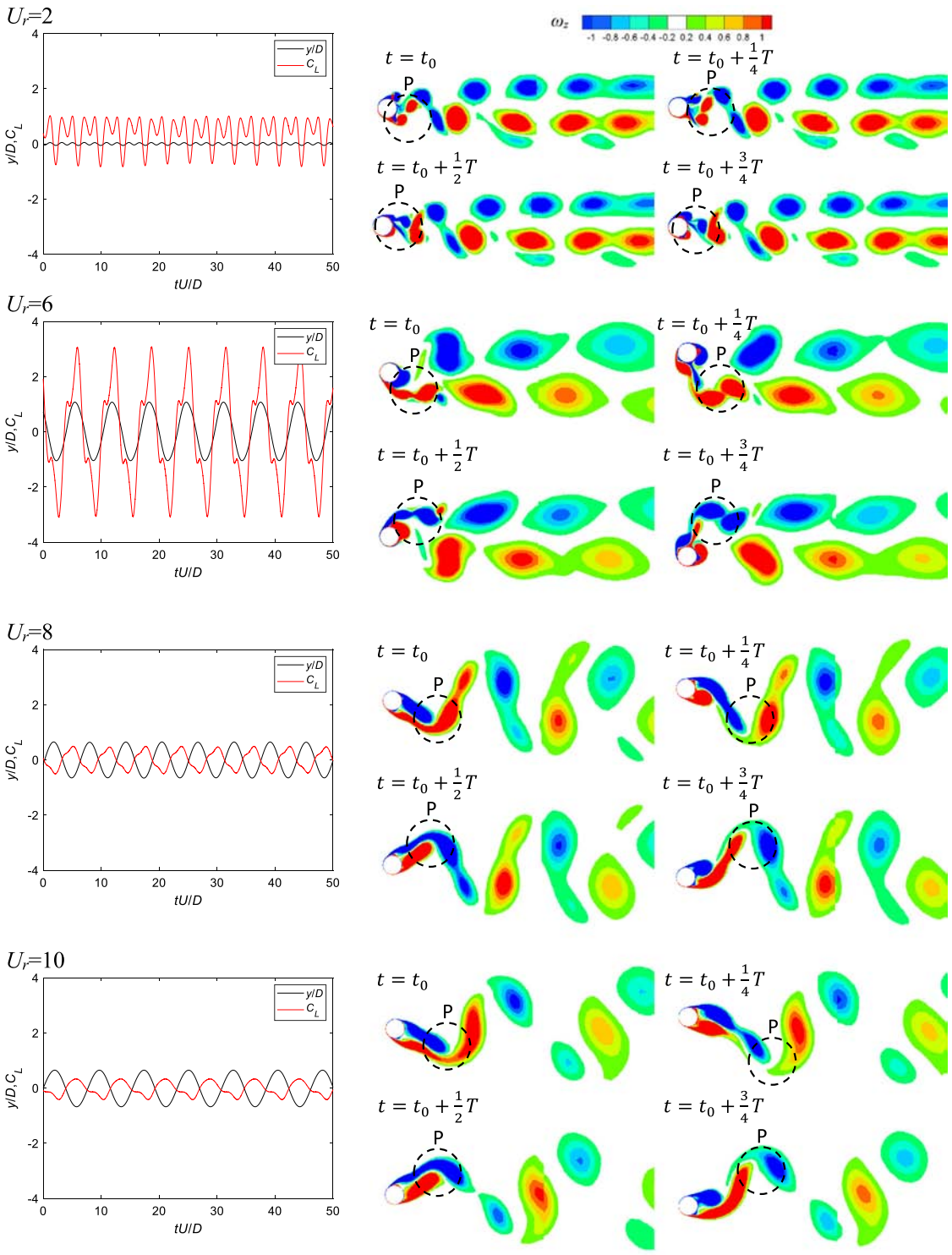

Fig. 7. Time history of transverse displacement y/D and lift coefficient C_L and contours of vorticity ω_z simulated by SST k-ω model for the circular cylinder with 2DOF linear system.

Fig. 4 illustrates the numerical results of mean drag coefficients $C_{D\ mean}$, fluctuating drag coefficients $C_{D\ rms}$, fluctuating lift coefficients $C_{L\ rms}$, non-dimensional vortex shedding frequency f_v/f_n and phase angle Φ between lift force and transverse displacement for the circular cylinder with 2DOF linear system. The mean drag coefficient $C_{D\ mean}$ and

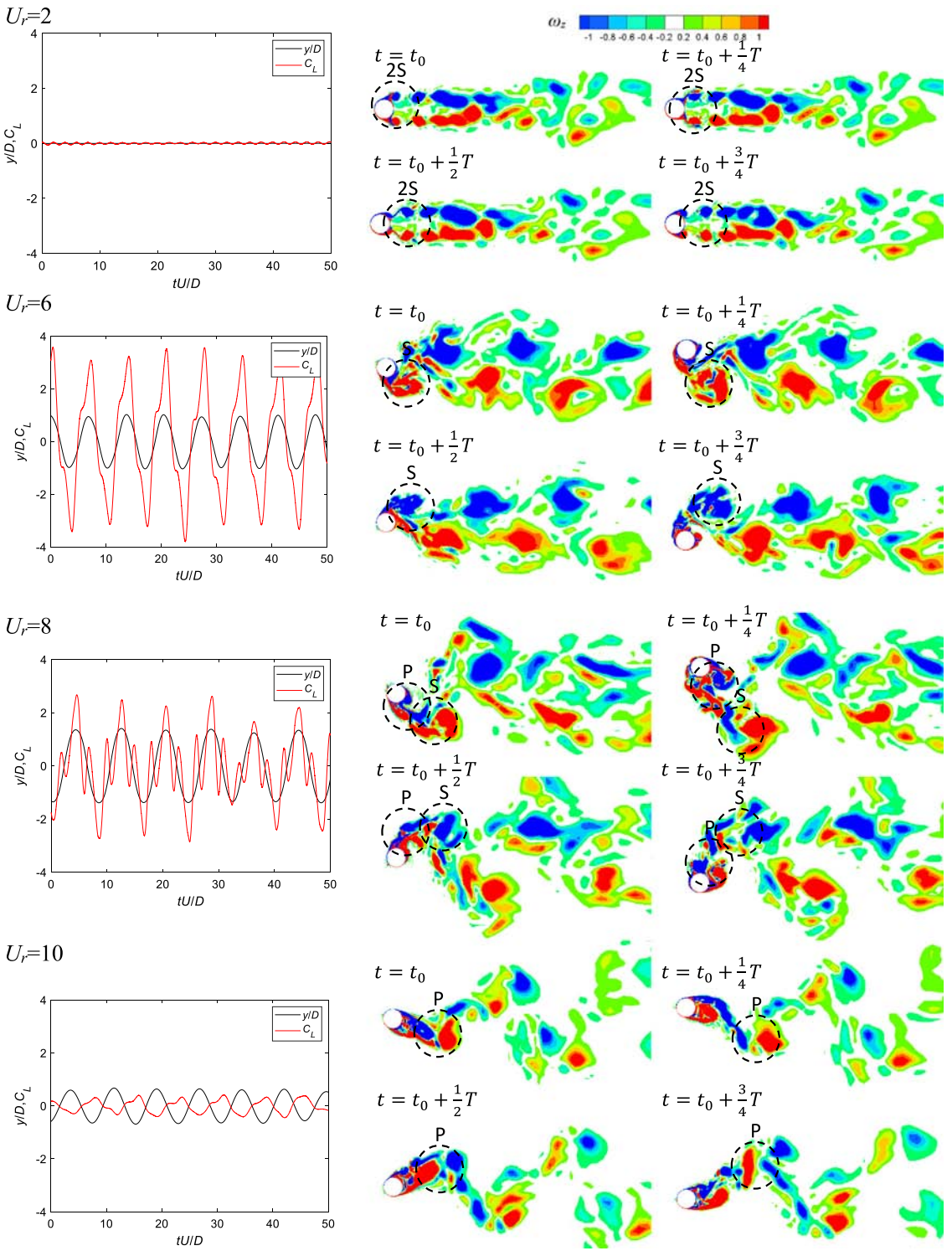

Fig. 8. Time history of transverse displacement y/D and lift coefficient C_L and contours of vorticity simulated by LES model for the circular cylinder with 2DOF linear system.

fluctuating drag coefficients $C_{D\,rms}$ are the mean value and root mean square error of drag coefficient $C_D = F_D/(0.5\rho U^2 DL)$. The fluctuating lift coefficient $C_{L\,rms}$ is the root mean square of lift coefficient $C_L = F_L/(0.5\rho U^2 DL)$. The vortex shedding

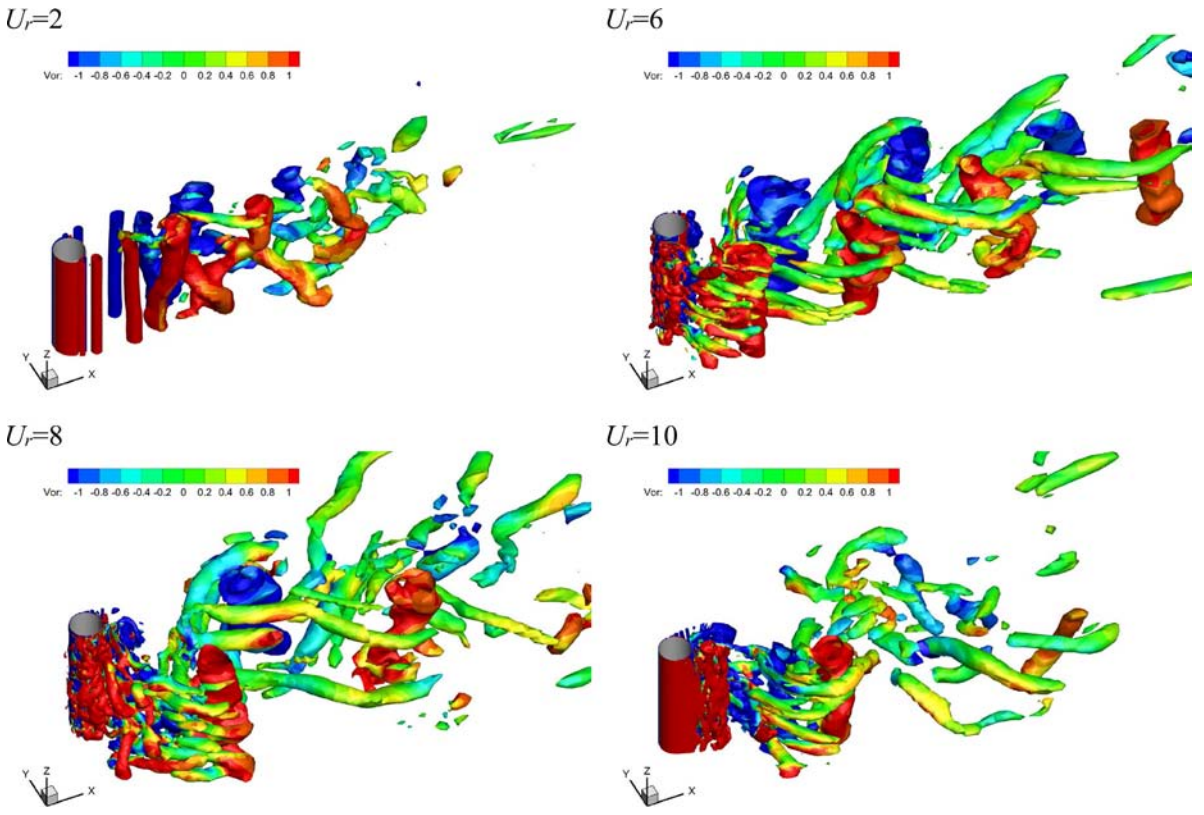

Fig. 9. The vortex cores around the circular cylinder with 2DOF linear system simulated by LES model.

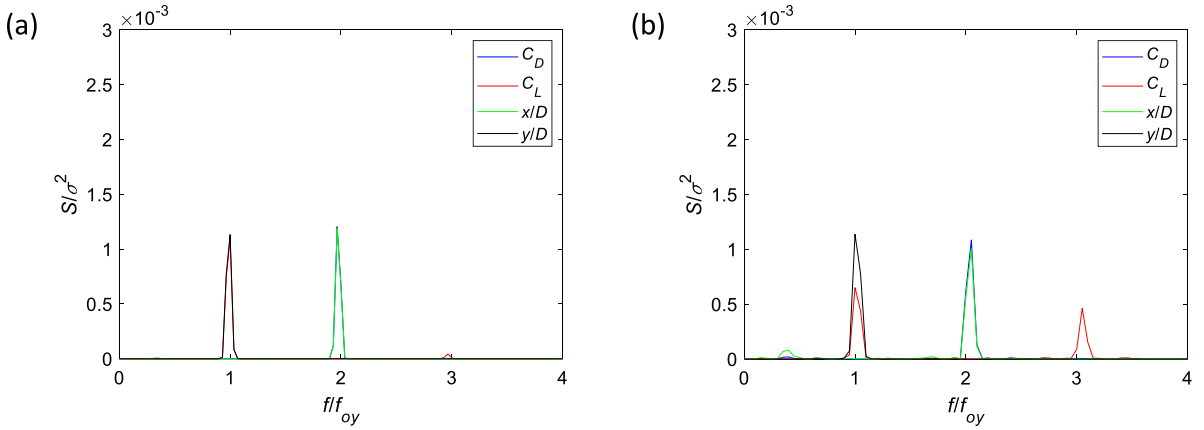

Fig. 10. Spectra of displacement and force coefficients of circular cylinder with 2DOF linear system simulated by (a) SST k-ω model and (b) LES model at $U_r = 8$.

frequency f_v is obtained by the spectrum analysis of lift force on cylinders. The experiment results of Jauvtis and Williamson (2004) are also shown in these figures for comparison. It can be seen that in the initial branch $C_{D\ mean}$ and $C_{L\ rms}$ increase with U_r, while $C_{D\ rms}$ decreases with U_r following the trend of streamwise vibration amplitude A_x. All of these three force coefficients increase with U_r in the upper branch and decrease with U_r in the super upper branch. After the transition from the super upper branch to the lower branch, they suddenly drop down and gradually decrease with U_r. The vortex shedding frequency f_v follows the constant St of about 0.22 in the unsympathetic region, while it keeps close to the structural natural frequency f_n in the sympathetic region, which shows an apparent "lock in" phenomenon. Particularly, f_v in the super upper branch has two dominating frequencies which will be discussed later. The phase angle Φ between lift force and transverse displacement is close to zero for $U_r \leq 8$ and change to about 180° for $U_r \geq 9$. The predicted

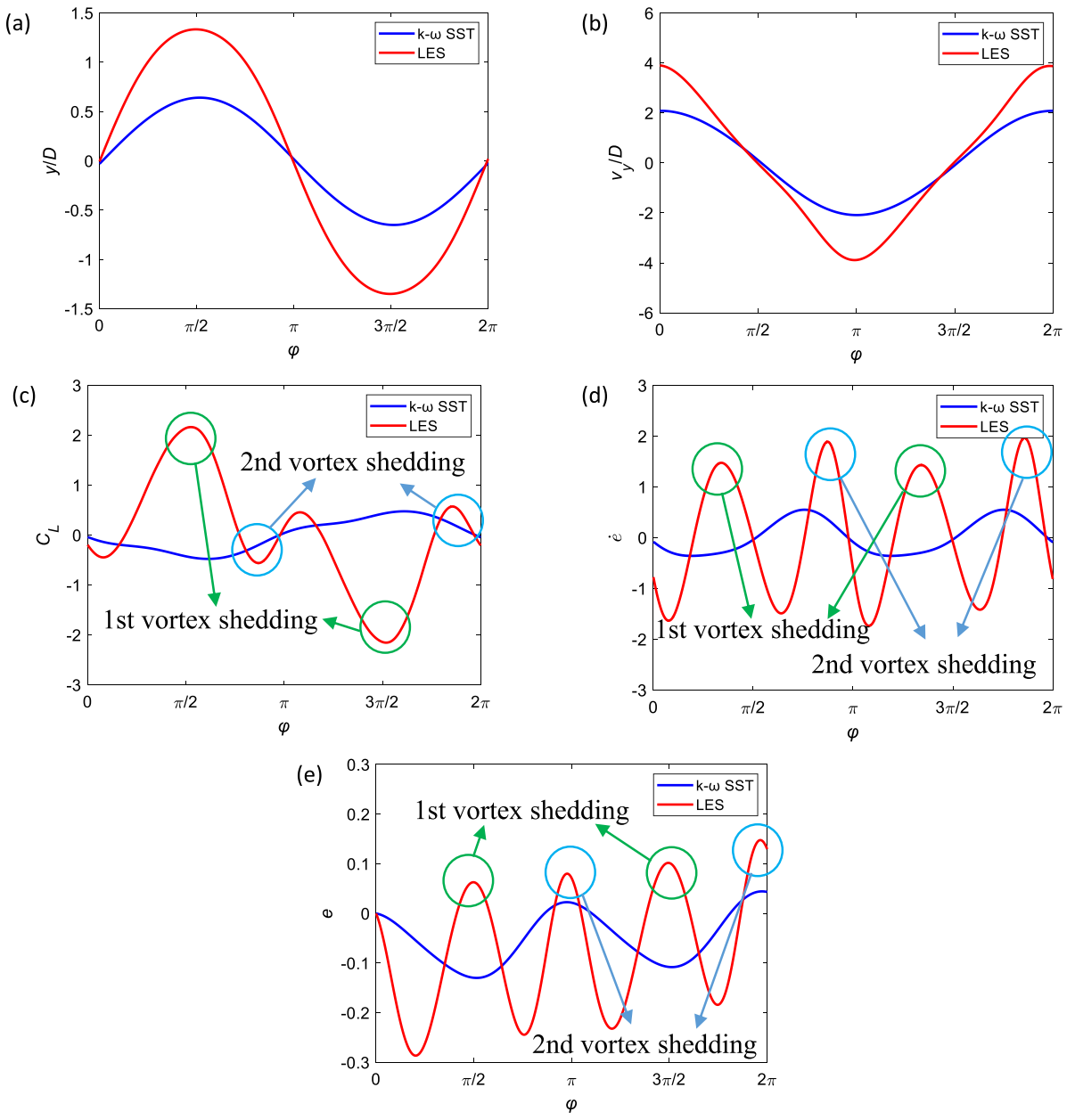

Fig. 11. Averaged (a) transverse displacement, (b) transverse velocity, (c) lift coefficient, (d) energy transfer rate and (e) energy transfer in one cycle of oscillation at $U_r = 8$ for the circular cylinder with 2DOF linear system.

$C_{D\ mean}$, $C_{D\ rms}$, $C_{L\ rms}$ and Φ by LES model agree well with the experiment data. The critical velocity of the transition from the super upper branch to the lower branch is underestimated by SST k-ω model.

The vibration trajectories and phase angles θ between streamwise and transverse motions simulated by SST k-ω and LES models are compared with the experiment results of Jauvtis and Williamson (2004) as shown in Figs. 5 and 6. It is found that the in-line-shaped and cross-line-shaped trajectories occur in the initial and lower branches respectively. Eight-shaped trajectory happens in the upper branch which is a typical trajectory of the 2DOF VIV of circular cylinder observed in the previous study (Blackburn and Karniadakis, 1993). The crescent-shaped trajectory happens in the super upper branch with the maximum vibration amplitude and indicates the phase angles θ between the streamwise and transverse motions is close to 270° (Jauvtis and Williamson, 2004). The vibration trajectories in different branches are well reproduced by LES model, however the crescent-shaped trajectory with the maximum vibration amplitude is failed to reproduce by SST k-ω model.

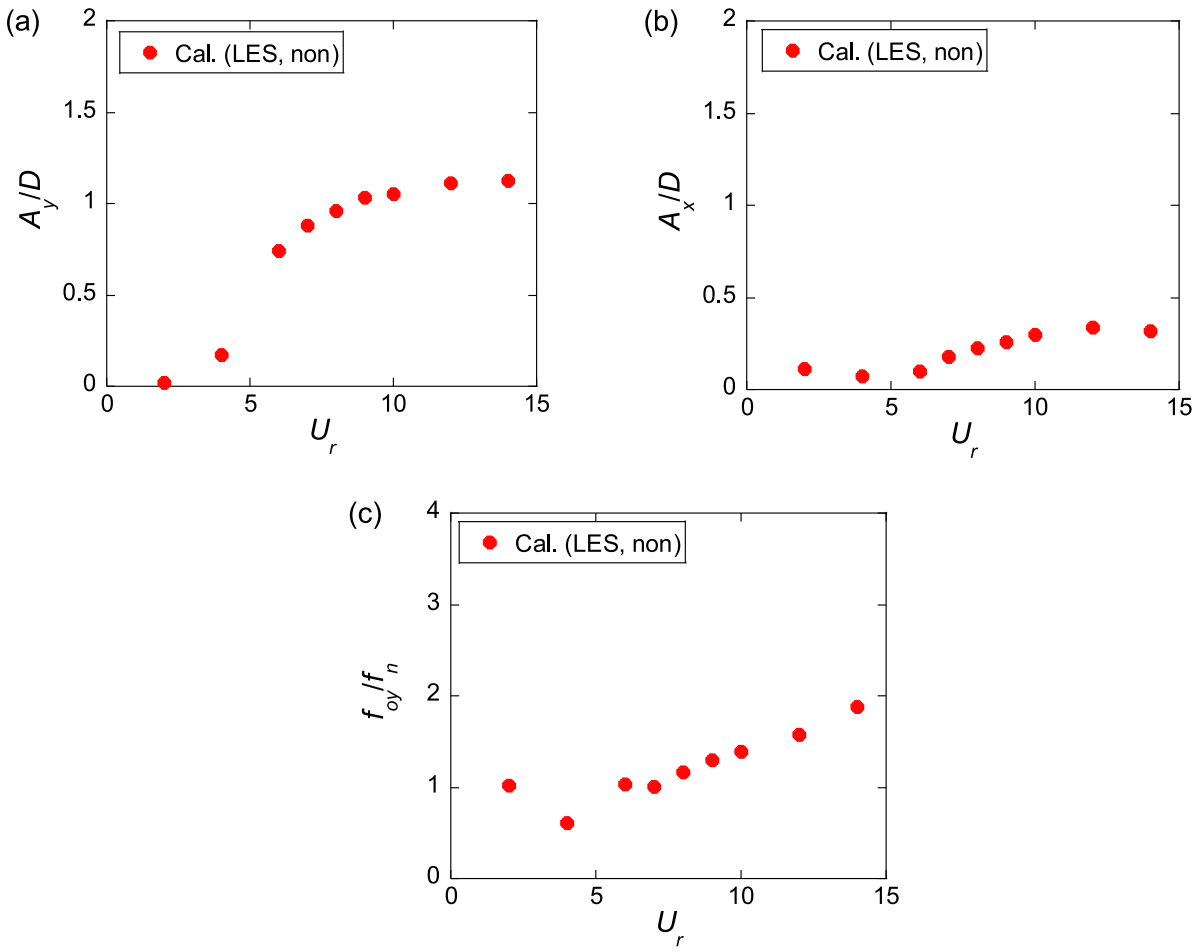

Fig. 12. Variation of (a) non-dimensional transverse amplitude A_y/D, (b) non-dimensional streamwise amplitude A_x/D and (c) non-dimensional transverse frequency f_{oy}/f_n of free vibration with U_r for circular cylinder with 2DOF nonlinear system.

The time history of non-dimensional transverse displacement y/D and lift coefficient C_L as well as the contours of non-dimensional spanwise vorticity ω_z for the circular cylinder with 2DOF linear system simulated by SST k-ω model are shown in Fig. 7, where ω_z is defined as $(\partial u_y/\partial x\text{-}\partial u_x/\partial y)/(U/D)$. Four different phases in a cycle of oscillation are presented with T standing for the period of oscillation and t_0 denoting the time when the cylinder is located in the balance position and has the positive velocity. The results of $U_r = 2$, 6, 8 and 10 are shown for example. It shows the simulated vortices with SST k-ω model are regular. Two pairs of uniform-sign vortices shed per cycle of oscillation and lead the in-phase y/D and C_L at $U_r = 2$ and 6. Two pairs of opposite-sign vortices shed per vibration period and lead the out-of-phase y/D and C_L at $U_r = 8$ and 10.

The time histories of non-dimensional displacement y/D and lift coefficient C_L as well as the contours of non-dimensional spanwise vorticity ω_z at the middle plane $z/L = 0.5$ for the circular cylinder with 2DOF linear system simulated by LES model are shown in Fig. 8. It is found that two parallel vortices shed per vibration period in the initial branches with $U_r = 2$ and form the side-by-side 2S vortex shedding mode. Two single vortices shed alternately in both sides of circular cylinder in the upper branches with $U_r = 6$ and form the 2S vortex shedding mode. At the super upper branch with $U_r = 8$, the maximum vibration amplitude occurs and the 2T vortex shedding mode forms. There are two large single vortices and two small vortex pairs shed alternately in a cycle of oscillation, which forms two triplets of vortices shedding per oscillation period. The two large single vortices lead large peaks of C_L when the circular cylinder reaches the maximum and minimum displacement, which is named as the first vortex shedding. The two small vortex pairs lead four small peaks of C_L when the circular cylinder passes the balance position, which is named as the second vortex shedding. The 2P vortex shedding mode appears in the lower branch with $U_r = 10$. The transition of vortex shedding mode from 2T to 2P leads the change of phase between y/D and C_L from in-phase to out-of-phase. The variation of vortex shedding mode with reduced velocity U_r simulated by LES model agrees well with the PIV experimental results of Jauvtis and Williamson (2004).

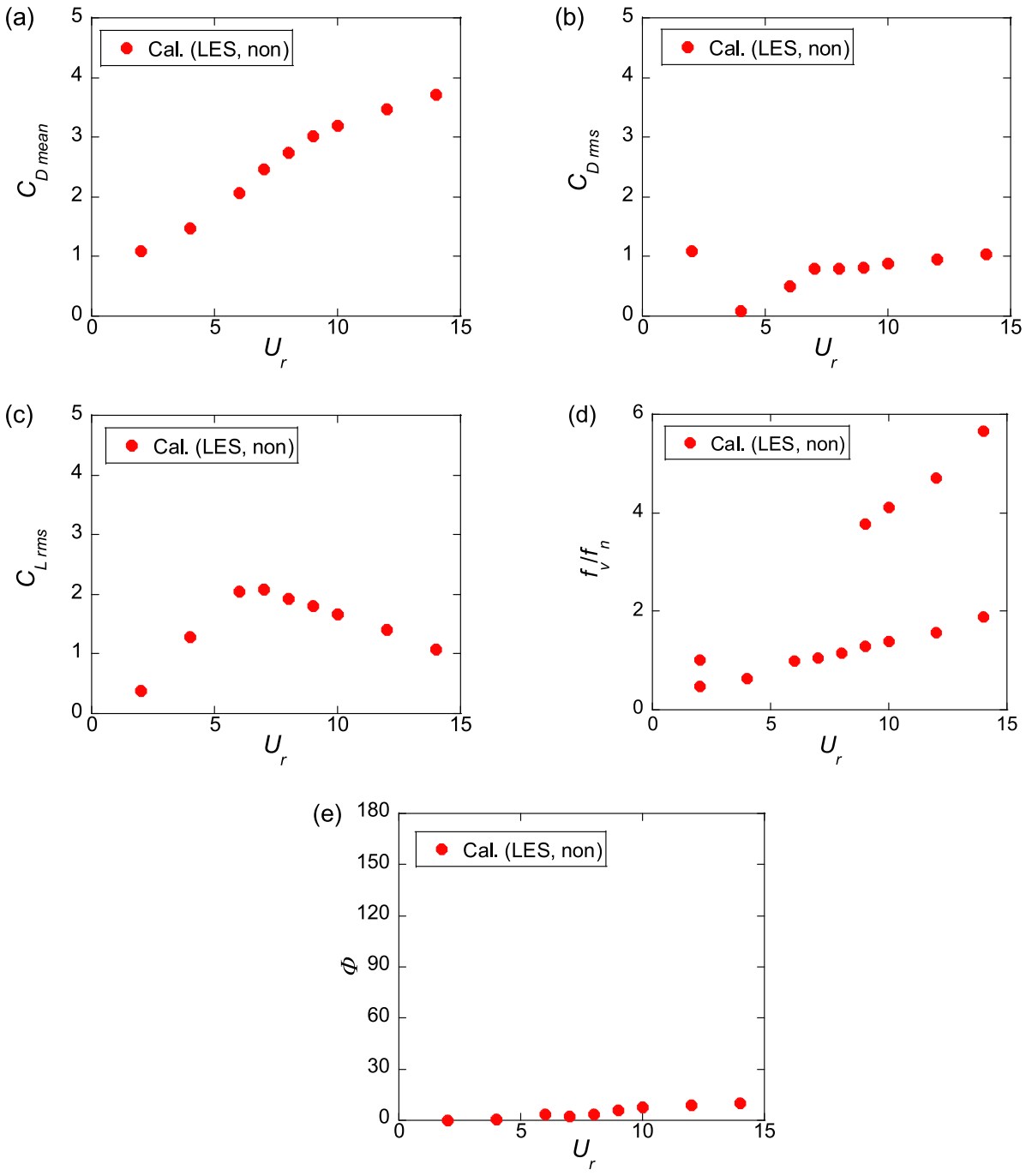

Fig. 13. Variation of (a) mean drag coefficients $C_{D\ mean}$, (b) fluctuating drag coefficients $C_{D\ rms}$, (c) fluctuating lift coefficients $C_{L\ rms}$, (d) non-dimensional vortex shedding frequency f_v/f_n and (e) phase angle Φ between lift force and transverse displacement with U_r for the circular cylinder with 2DOF nonlinear system.

The vortex cores around the circular cylinder with 2DOF linear system simulated by LES model are shown in Fig. 9. The vortex cores are visualized by iso-surfaces of the non-dimensional second negative eigenvalue e_2 of the tensor $\tilde{S}^2 + \tilde{\Omega}^2$ using the method proposed by Jeong and Hussain (1995). $e_2 = \lambda_2/(U/D)^2$ is set as -0.2 with λ_2 being the dimensional second negative eigenvalue of the tensor $\tilde{S}^2 + \tilde{\Omega}^2$. $\tilde{S}$ and $\tilde{\Omega}$ are the symmetric and antisymmetric components of the

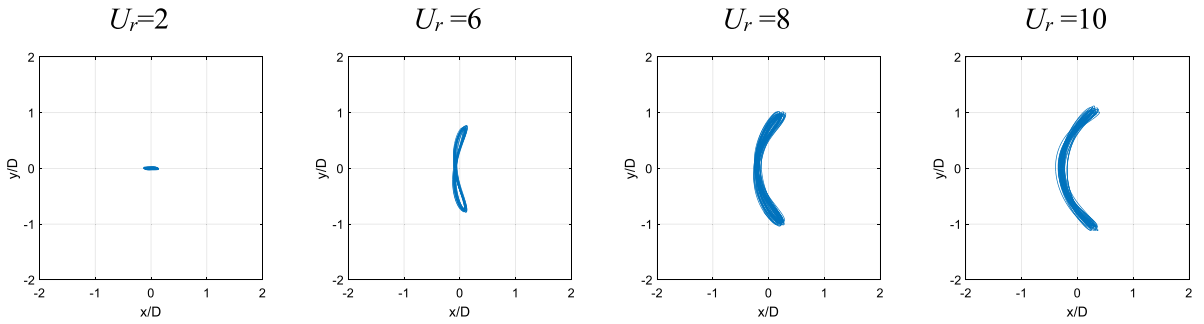

Fig. 14. Vibration trajectory of circular cylinder with 2DOF nonlinear system.

velocity-gradient tensor $\nabla\tilde{u}$. $\tilde{S}_{ij}$ is defined in Eq. (5) and $\tilde{\Omega}_{ij}$ is expressed as

$$\tilde{\Omega}_{ij} = \frac{1}{2}\left(\frac{\partial \tilde{u}_i}{\partial x_j} - \frac{\partial \tilde{u}_j}{\partial x_i}\right) \tag{14}$$

These iso-surfaces are coloured by the non-dimensional spanwise vorticity ω_z and are at the transient time $t = t_0 + T/4$ when the cylinder gets the maximum transverse displacement. It is found that in the initial branch with $U_r = 2$ the vortices shed from the cylinder are relatively two-dimensional in the near wake and more three-dimensional in the far wake. The centre lines of the vortices are almost parallel to the cylinder in the near wake, but inclined in the far wake. In the upper branch with $U_r = 6$, the wake is the strongest and the regular Karman vortex street is the longest. As a result, $C_{D\,rms}$ and $C_{L\,rms}$ reach the maximum values. At the super upper branch with $U_r = 8$, the three-dimensionality of flow field is quite strong due to the 2T vortex shedding mode and the centre lines of the vortices are inclined in the near wake of cylinder, so that $C_{D\,rms}$ and $C_{L\,rms}$ are smaller than those at $U_r = 6$. In the lower branch with $U_r = 10$, a short wake forms and leads small $C_{D\,rms}$ and $C_{L\,rms}$.

The spectra of non-dimensional streamwise displacement x/D, non-dimensional transverse displacement y/D, drag coefficient C_D and lift coefficient C_L of circular cylinder with 2DOF linear system simulated by SST k-ω model and LES model at $U_r = 8$ with the peak vibration amplitude are shown in Fig. 10. It is found that in the results with LES model x/D, y/D and C_D are generally harmonic with one dominating frequency of f_{oy}. C_L has two dominating frequencies of f_{oy} and $3f_{oy}$, and the f_{oy} component of C_L is larger than the $3f_{oy}$ component, same as the experimental phenomenon of Jauvtis and Williamson (2004). Combining with the time history of C_L shown in Fig. 8, it can be seen that the f_{oy} component of C_L corresponds the first vortex shedding and the $3f_{oy}$ component is caused by the second vortex shedding. The peaks of spectra of x/D and C_D are almost same and located at $2f_{oy}$. In the simulation with SST k-ω model, the $3f_{oy}$ component of C_L is negligible because the second vortex shedding cannot be simulated successfully.

The energy transfer from the fluid to the circular cylinder is analysed based on the numerical results with SST k-ω model and LES model according to the research of Jauvtis and Williamson (2004) and Carberry et al. (2005). The averaged transverse displacement y/D, transverse velocity v_y/D, lift coefficient C_L, energy transfer rate $\dot{e}$ and energy transfer e in one cycle of oscillation at the super upper branch with $U_r = 8$ are shown in Fig. 11, where the energy transfer rate $\dot{e}$ is defined as $\dot{e} = C_L \cdot \dot{y}/D$ and the energy transfer e is calculated by $e = \int_0^T \dot{e}dt$. In the LES study, the first vortex shedding happens when the cylinder reaches the maximum and minimum transverse displacement and the second vortex shedding happens when the cylinder passes the balance position, which leads peak values of C_L. As the y/D and C_L are in-phase, the positive energy transfer rate from the fluid to the cylinder is generated just before the vortex shedding and happens four times in one cycle of oscillation. As a result, the total energy transfer from the fluid to the cylinder is positive and has a large magnitude, which leads the large vibration amplitude. In the simulation by SST k-ω model, there is only the first vortex shedding. As the y/D and C_L are out-of-phase, the positive energy transfer rate from the fluid to the cylinder is generated just after the vortex shedding and happens two times in one period of oscillation. The total energy transfer from the fluid to the cylinder is positive but small, which leads the smaller vibration amplitude than the one of LES results. In addition, in the SST k-ω simulation the positive energy transfer rate occurs when the cylinder is approaching the balance position and has large velocity. Therefore, even the $C_{L\,rms}$ is small, the energy transfer rate is still considerable and leads significant vibration amplitude.

4. VIV of circular cylinder with 2DOF nonlinear system

The free-vibration of circular cylinder with 2DOF nonlinear system under the reduced velocity U_r from 2 to 14 is simulated by increasing U_r with a step of 2. A smaller step of 1 is used near $U_r = 6\sim10$, being consistent with that for the 2DOF linear system. Both f_n and D are fixed, while U is varied to change U_r in these simulations, resulting in $Re = 2000\sim14\,000$. The predicted non-dimensional transverse and streamwise vibration amplitudes A_y/D and A_x/D as well as the non-dimensional transverse vibration frequency f_{oy}/f_n of circular cylinder simulated by LES model are shown in

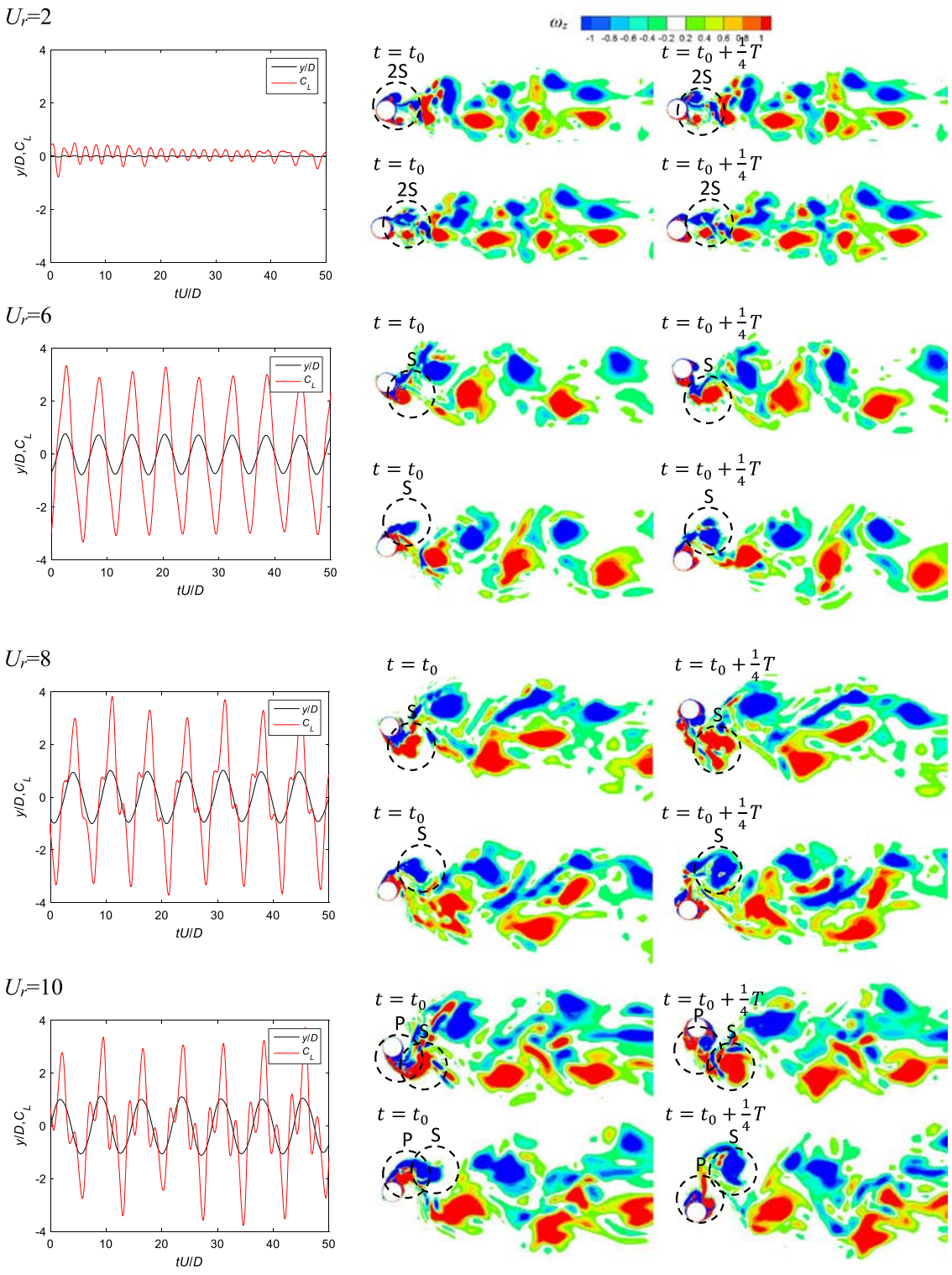

Fig. 15. Time history of transverse displacement and lift coefficients and contours of vorticity simulated with LES model for the circular cylinder with 2DOF nonlinear system.

Fig. 12. It is found that both streamwise and transverse vibration amplitudes of circular cylinder with 2DOF nonlinear system increase with the reduced velocity U_r and approach asymptotes at high U_r, similar to the classic galloping. This

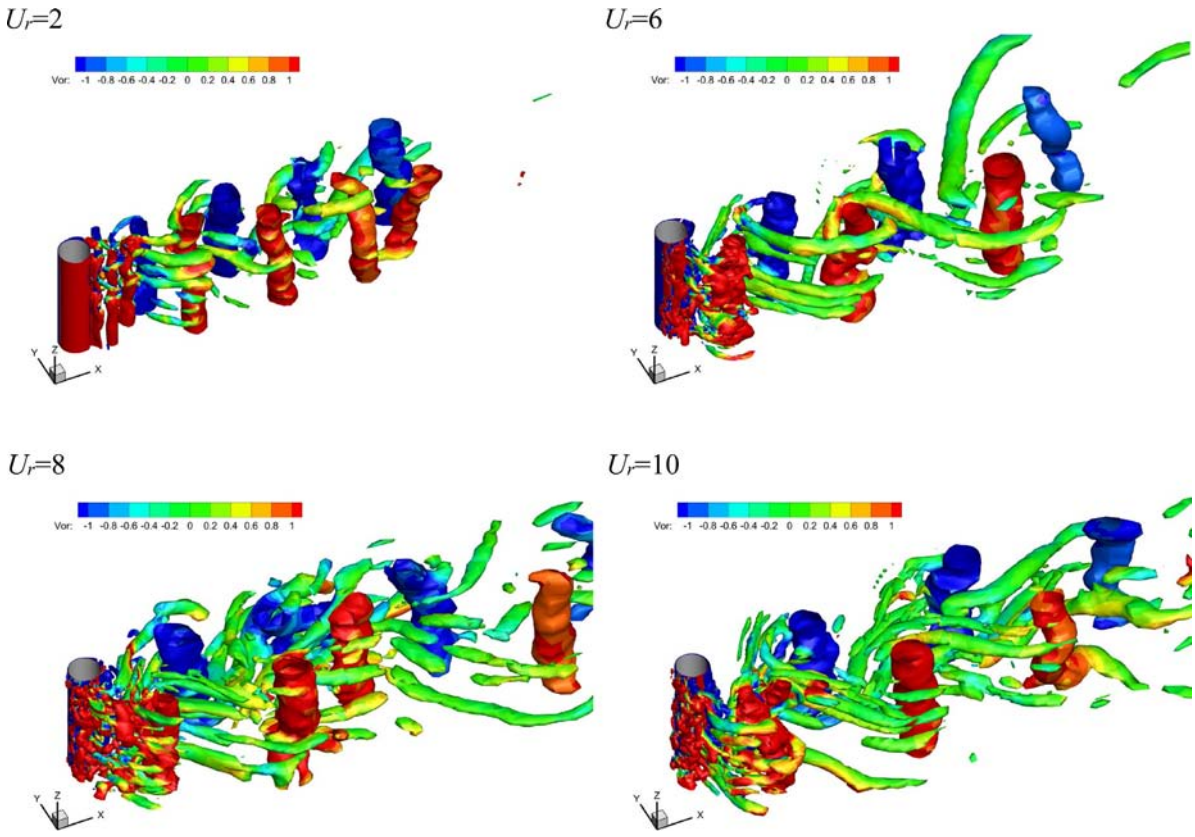

Fig. 16. The vortex cores around the circular cylinder with 2DOF nonlinear system simulated by LES model.

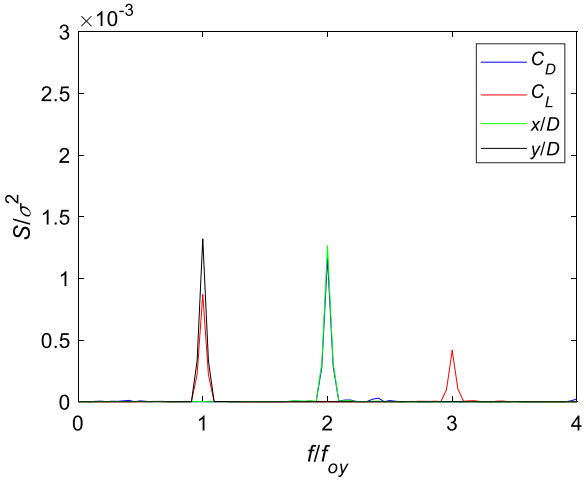

Fig. 17. Spectra of displacement and force coefficients of circular cylinder with 2DOF nonlinear system simulated by LES model at $U_r = 10$.

phenomenon was also found by Mackowski and Williamson (2013) and Huynh et al. (2015) through the experiments with nonlinear circular cylinders. The transverse vibration frequency f_{oy} of cylinder with 2DOF nonlinear system also continues to increase with the reduced velocity U_r even at a high U_r.

Fig. 13 illustrates the numerical results of mean drag coefficients $C_{D\ mean}$, fluctuating drag coefficients $C_{D\ rms}$, fluctuating lift coefficients $C_{L\ rms}$, non-dimensional vortex shedding frequency f_v/f_n and phase angle Φ between lift force and transverse displacement for the circular cylinder with 2DOF nonlinear system. It is found that $C_{D\ mean}$ and $C_{D\ rms}$ generally increase with U_r, which is distinguished with the results of circular cylinder with 2DOF linear system. $C_{L\ rms}$ shows a

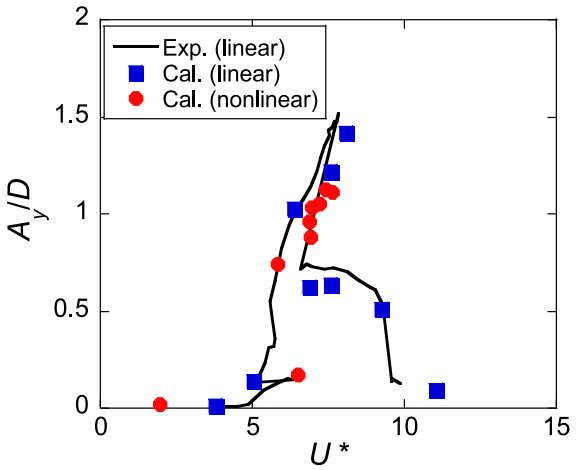

Fig. 18. Variation of non-dimensional transverse amplitude A_y/D of circular cylinder with U^*.

convergent pattern, but remains significant at high U_r. The f_v has two dominating frequencies upon $U_r = 9$. The lift force and transverse displacement are always in-phase for the cylinder with nonlinear system.

The predicted vibration trajectory of the circular cylinder with 2DOF nonlinear system is shown in Fig. 14. It is found that the in-line-shaped and eight-shaped trajectories occur at $U_r = 2$, 6 and 8 respectively, which are similar to those with 2DOF linear system. However, the trajectory keeps as the crescent-shape when U_r is larger than 9, which indicates the phase angle between the streamwise and transverse directions tends to 270° as U_r increases.

The time histories of non-dimensional displacement y/D and lift coefficient C_L as well as the contours of non-dimensional spanwise vorticity ω_z at different phases in a cycle of oscillation for the circular cylinder with 2DOF nonlinear system simulated by LES model are shown in Fig. 15. The results of $U_r = 2$, 6, 8 and 10 are shown for example. It is found at the reduced velocity $U_r = 2$, the side-by-side 2S vortex shedding pattern forms and then changes to the staggered 2S mode. As U_r increases, the vortex shedding mode changes to the 2S mode at $U_r = 6$ and 8. The 2T mode forms at $U_r = 9$ and keeps until the simulated maximal reduced velocity $U_r = 14$. The characteristics of y/D, C_L and ω_z at $U_r = 9\sim14$ for the circular cylinder with 2DOF nonlinear system are similar to those in the super upper branch of cylinder with 2DOF linear system.

The vortex core around the circular cylinder with 2DOF nonlinear system simulated by LES model are shown in Fig. 16. At the reduced velocity $U_r = 2\sim8$, the near wake after the cylinder is relatively two-dimensional, which is similar to the ones in the initial and upper branch of the cylinder with 2DOF linear system. As U_r increases, the vortex shedding mode changes to the 2T mode from $U_r = 9$ and keeps as the 2T mode until the simulated maximum $U_r = 14$. The three-dimensionalities are quite significant in the near wake and the centre lines of vortex cores are inclined to the cylinder for $U_r = 9\sim14$, which is also similar to the phenomenon in the super upper branch of cylinder with 2DOF linear system.

The spectra of non-dimensional streamwise displacement x/D, non-dimensional transverse displacement y/D, drag coefficient C_D and lift coefficient C_L simulated by LES model for the circular cylinder with 2DOF nonlinear system at $U_r = 10$ are shown in Fig. 17. It is seen that x/D, y/D and C_D are generally harmonic with one dominating frequency. C_L has two dominating frequencies including f_{oy} component and $3f_{oy}$ component, which is similar with the phenomenon in the super upper branch of circular cylinder with 2DOF linear system. The dominating frequency of x/D and C_D are same and located at the twice of transverse vibration frequency f_{oy}.

The nonlinearity defined in this research makes the nonlinear system stiffer than the linear system, and the stiffness increases with the vibration amplitude. As a result, the transverse vibration frequency f_{oy} increases with the reduced velocity U_r as shown in Fig. 12. The variation of non-dimensional transverse vibration amplitude A_y/D of circular cylinder with a modified reduced velocity U^* is shown in Fig. 18, where U^* is defined as

$$U^* = \frac{U}{f_{oy}D} \tag{15}$$

It is found that the responses of linear and nonlinear cylinders share the same rule. With the increasing inflow velocity, the transverse vibration frequency f_{oy} of nonlinear cylinder increases and makes the U^* increase slowly or even keep constant. As a result, the nonlinear cylinder keeps in the super upper branch in a wide range of velocity. It means the galloping-like vibration of the nonlinear circular cylinder is induced by the amplitude-dependent stiffness of system. The relationship of the modified reduced velocity U^* and vibration amplitude is insensitive to the nonlinearity of the cylinder system and U^* is a more universal variable to describe the vibration characteristics than U_r.

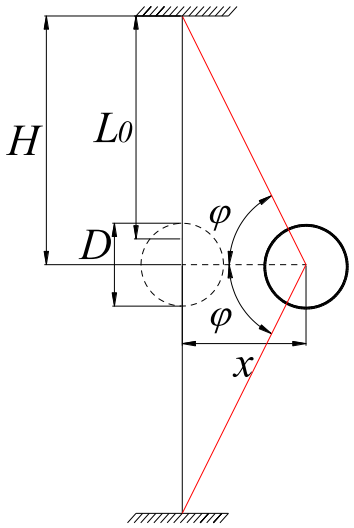

Fig. A.1. Schematic of geometrical nonlinear system.

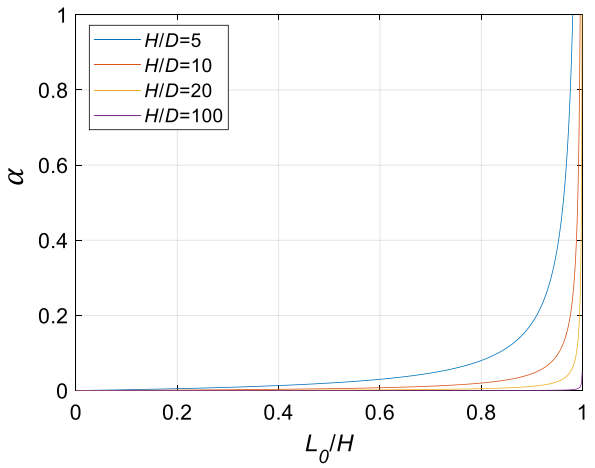

Fig. A.2. Variation of geometrical nonlinear coefficient α with L_0/H for different H/D.

5. Conclusions

The vortex-induced vibration of circular cylinder in uniform flow with two-degree-of-freedom and geometrical nonlinear system is investigated using SST k-ω and LES turbulence models. The characteristics of vibration amplitude, fluid force coefficient, branching behaviour, vibration trajectory, energy transfer and vortex shedding mode of circular cylinder in VIV are investigated. The main conclusions are as follows:

(1) The vibration amplitude, fluid force coefficient, branching behaviour, vibration trajectory and vortex shedding mode of circular cylinder with 2DOF linear system in VIV are well reproduced by the LES turbulence model, while the maximum vibration amplitude is underestimated and the super upper branch of VIV cannot be reproduced by the SST k-ω model.

(2) In the super upper branch of VIV for the circular cylinder with 2DOF linear system, the 2T vortex shedding mode happens and leads f_{oy} and $3f_{oy}$ components of lift force, which are related to the first and second vortex shedding respectively. The second vortex shedding increases the energy transfer from the fluid to the cylinder and causes the maximum vibration amplitude.

(3) The vibration amplitude keeps increasing with the reduced velocity U_r and shows a galloping-like phenomenon for the circular cylinder with 2DOF nonlinear system. The vibration characteristics of circular cylinder with 2DOF nonlinear system at high velocity are similar to that in the super upper branch of cylinder with 2DOF linear system. This phenomenon is induced by the amplitude-dependent stiffness of system and the variation of vibration amplitude with the modified reduced velocity U^* is universal for the circular cylinder with linear and nonlinear systems.

CRediT authorship contribution statement

Tian Li: Data curation, Conceptualization, Formal analysis, Methodology, Investigation, Software, Validation, Visualization, Writing – original draft, Writing – review & editing. **Takeshi Ishihara:** Conceptualization, Formal analysis, Funding acquisition, Methodology, Project administration, Resources, Supervision, Writing – review & editing.

Declaration of competing interest

The authors declare that they have no known competing financial interests or personal relationships that could have appeared to influence the work reported in this paper.

Acknowledgements

The authors wish to thank the 111 Project of China (Grant No. B18062) and the Postdoctoral Research Foundation of China (Grant No. 2021M693737) for the funding support.

Appendix. Derivation of duffing equation considering geometrical nonlinearity

The circular cylinder of mass m is connected to the fixed boundary by the linear spring of negligible mass as shown in Fig. A.1. The natural length of each spring is L_0 and the spring constant is Λ. The distance between cylinder and boundary is H where $H > L_0$.

When the cylinder is displaced horizontally with a distance x, the restoring force F equals

$$F = \Lambda\left(\frac{\sqrt{H^2+x^2}-L_0}{L_0}\right) \tag{A.1}$$

Newton's second law and $\cos\varphi = \frac{x}{\sqrt{H^2+x^2}}$ yield

$$m\frac{d^2x}{dt^2} = -2F\cos\varphi = -\frac{2\Lambda}{L_0}x\left(1-\frac{L_0}{\sqrt{H^2+x^2}}\right) \tag{A.2}$$

When the displacement x is small compared with H, the inverse square root term may be replaced by a truncated Maclaurin expansion. On keeping two terms in the expansion, it is obtained as

$$\frac{d^2x}{dt^2} = -\frac{2\Lambda}{mL_0}x\left[1-\frac{L_0}{H}\left(1-\frac{1}{2}\frac{x^2}{H^2}\right)\right] \tag{A.3}$$

Introducing the nondimensional displacement $X = x/D$ and the frequency related parameter $\Omega = \sqrt{\frac{2\Lambda(H-L_0)}{mL_0H}}$, the governing equation becomes

$$\frac{d^2X}{dt^2} = -\Omega^2\left[X+\frac{L_0}{2(H-L_0)}\frac{D^2}{H^2}X^3\right] \tag{A.4}$$

Then on introducing nondimensional time $\tau = \Omega t$ and the geometrical nonlinear coefficient $\alpha = \frac{L_0D^2}{2(H-L_0)H^2}$, the Duffing equation is obtained as

$$\frac{d^2X}{d\tau^2} + X + \alpha X^3 = 0 \tag{A.5}$$

If setting the parameters as $\gamma = L_0/H$ and $\eta = H/D$, it yields $\alpha = \frac{\gamma}{2(1-\gamma)\eta^2}$. The relationship between α and L_0/H for different H/D is shown in Fig. A.2. It is found that the geometrical nonlinearity is significant when L_0 is close to H.

When the geometrical nonlinear coefficient $\alpha = 0.7$ is assumed as mentioned by Srinil and Zanganeh (2012), the relationship between γ and η is expressed as

$$\gamma = \frac{1.4\eta^3}{1+1.4\eta^2} \tag{A.6}$$

Fig. A.3 shows the relationship between L_0/D and H/D. It is obvious that $\alpha = 0.7$ is a good approximation when L_0 is long compared with D and close to H.

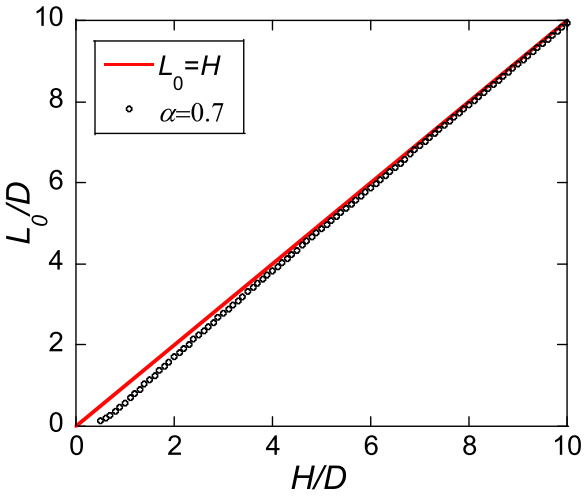

Fig. A.3. The relationship between L_0/D and H/D.

References

ANSYS Inc., 2015. ANSYS FLUENT 16.2 theory guide.

Bernitsas, M.M., Raghavan, K., Ben-Simon, Y., Garcia, E., 2008. VIVACE (vortex induced vibration aquatic clean energy): A new concept in generation of clean and renewable energy from fluid flow. J. Offshore Mech. Arct. Eng. 130, 041101.

Blackburn, H.M., Karniadakis, G.E., 1993. Two- and three-dimensional simulations of vortex-induced vibration of a circular cylinder, in: 3rd International Offshore and Polar Engineering Conference, Singapore, 3, pp. 715-720.

Bush, A.W., 1992. Perturbation Methods for Engineers and Scientists. CRC Press.

Carberry, J., Sheridan, J., Rockwell, D., 2005. Controlled oscillations of a cylinder: forces and wake modes. J. Fluid Mech. 538 (31).

Feng, C.C., 1968. The Measurement of Vortex Induced Effects in Flow Past Stationary and Oscillating Circular and D-Section Cylinders (Master dissertation). University of British Columbia.

Ferziger, J.H., Peric, M., 2002. Computational Methods for Fluid Dynamics. Springer Science & Business Media.

Germano, M., Piomelli, U., Moin, P., Cabot, W.H., 1991. A dynamic subgrid-scale eddy viscosity model. Phys. Fluids A 3 (7), 1760–1765.

Griffin, O.M., 1980. Vortex-excited cross-flow vibrations of a single cylindrical tube. J. Press. Vessel Technol. 102 (2), 158–166.

Gsell, S., Bourguet, R., Braza, M., 2016. Two-degree-of-freedom vortex-induced vibrations of a circular cylinder at Re = 3900. J. Fluids Struct. 67, 156–172.

Guilmineau, E., Queutey, P., 2004. Numerical simulation of vortex-induced vibration of a circular cylinder with low mass-damping in a turbulent flow. J. Fluids Struct. 19 (4), 449–466.

Huynh, B.H., Tjahjowidodo, T., Zhong, Z.W., Wang, Y., Srikanth, N., 2015. Nonlinearly enhanced vortex induced vibrations for energy harvesting. In: 2015 IEEE International Conference on Advanced Intelligent Mechatronics. pp. 91–96.

Ishihara, T., Li, T., 2020. Numerical study on suppression of vortex-induced vibration of circular cylinder by helical wires. J. Wind Eng. Ind. Aerodyn. 197, 104081.

Jauvtis, N., Williamson, C.H.K., 2004. The effect of two degrees of freedom on vortex-induced vibration at low mass and damping. J. Fluid Mech. 509, 23–62.

Jeong, J., Hussain, F., 1995. On the identification of a vortex. J. Fluid Mech. 285, 69–94.

Khalak, A., Williamson, C.H.K., 1996. Dynamics of a hydroelastic cylinder with very low mass and damping. J. Fluids Struct. 10 (5), 455–472.

Khalak, A., Williamson, C.H.K., 1997. Fluid forces and dynamics of a hydroelastic structure with very low mass and damping. J. Fluids Struct. 11 (8), 973–982.

Khalak, A., Williamson, C.H., 1999. Motions, forces and mode transitions in vortex-induced vibrations at low mass-damping. J. Fluids Struct. 13 (7–8), 813–851.

Leontini, J.S., Thompson, M.C., Hourigan, K., 2006. The beginning of branching behaviour of vortex-induced vibration during two-dimensional flow. J. Fluids Struct. 22 (6–7), 857–864.

Li, T., Ishihara, T., 2021. Numerical study on wake galloping of tandem circular cylinders considering the effects of mass and spacing ratios. J. Wind Eng. Ind. Aerodyn. 210, 104536.

Li, T., Yang, Q., Ishihara, T., 2018. Unsteady aerodynamic characteristics of long-span roofs under forced excitation. J. Wind Eng. Ind. Aerodyn. 181, 46–60.

Lilly, D.K., 1992. A proposed modification of the germano subgrid scale closure method. Phys. Fluids A 4 (3), 633–635.

Lucor, D., Foo, J., Karniadakis, G.E., 2005. Vortex mode selection of a rigid cylinder subject to VIV at low mass-damping. J. Fluids Struct. 20 (4), 483–503.

Mackowski, A.W., Williamson, C.H.K., 2013. An experimental investigation of vortex-induced vibration with nonlinear restoring forces. Phys. Fluids 25 (8), 355–381.

Menter, F.R., 1994. Two-equation eddy-viscosity turbulence models for engineering applications. AIAA J. 32 (8), 1598–1605.

Navrose, Mittal, S., 2013. Free vibrations of a cylinder: 3-D computations at Re = 1000. J. Fluids Struct. 41, 109–118.

Pan, Z.Y., Cui, W.C., Miao, Q.M., 2007. Numerical simulation of vortex-induced vibration of a circular cylinder at low mass-damping using RANS code. J. Fluids Struct. 23 (1), 23–37.

Pontaza, J.P., Chen, H.C., 2007. Three-dimensional numerical simulations of circular cylinders undergoing two degree-of-freedom vortex-induced vibrations. ASME J. Offshore Mech. Arct. Eng. 129, 158–164.

Saltara, F., Neto, A.A., Lopez, J.I.H., 2011. 3D CFD simulation of vortex-induced vibration of cylinder. Int. J. Offshore Polar Eng. 21 (03).

Sarwar, M.W., Ishihara, T., 2010. Numerical study on suppression of vortex-induced vibrations of box girder bridge section by aerodynamic countermeasures. J. Wind Eng. Ind. Aerodyn. 98 (12), 701–711.
Singh, S.P., Mittal, S., 2005. Vortex-induced oscillations at low Reynolds numbers: hysteresis and vortex-shedding modes. J. Fluids Struct. 20 (8), 1085–1104.
Smagorinsky, J., 1963. General circulation experiments with the primitive equations: I. The basic experiment. Mon. Weather Rev. 91 (3), 99–164.
Srinil, N., Zanganeh, H., 2012. Modelling of coupled cross-flow/in-line vortex-induced vibrations using double duffing and van der pol oscillators. Ocean Eng. 53, 83–97.
Wang, W., Mao, Z., Tian, W., T., Zhang., 2019. Numerical investigation on vortex-induced vibration suppression of a circular cylinder with axial-slats. J. Mar. Sci. Eng. 7 (454).
Willden, R.H.J., Graham, J.M.R., 2006. Three distinct response regimes for the transverse vortex-induced vibrations of circular cylinders l at low Reynolds numbers. J. Fluids Struct. 22 (6–7), 885–895.
Williamson, C.H.K., 1988. The existence of two stages in the transition to three-dimensionality of a cylinder wake. Phys. Fluids 31, 3165–3168.
Williamson, C.H.K., Roshko, A., 1988. Vortex formation in the wake of an oscillating cylinder. J. Fluids Struct. 2 (4), 355–381.
Zhang, S., Ishihara, T., 2018. Numerical study of hydrodynamic coefficients of multiple heave plates by large eddy simulations with volume of fluid method. Ocean Eng. 163, 583–598.
Zhao, M., Cheng, L., 2011. Numerical simulation of two degree of freedom vortex-induced vibration of a circular cylinder close to a plane boundary. J. Fluids Struct. 27, 1097–1110.
Zhao, M., Cheng, L., An, H., Lu, L., 2014. Three-dimensional numerical simulation of vortex-induced vibration of an elastically mounted rigid circular cylinder in steady current. J. Fluids Struct. 50, 292–311.